

# Synthesis and Characterization of Boron-Doped Single-Wall Carbon Nanotubes Produced by the Laser Vaporization Technique

Jeff L. Blackburn,<sup>\*,†</sup> Yanfa Yan,<sup>†</sup> Chaiwat Engtrakul,<sup>†</sup> Philip A. Parilla,<sup>†</sup> Kim Jones,<sup>†</sup> Thomas Gennett,<sup>‡</sup> Anne C. Dillon,<sup>†</sup> and Michael J. Heben<sup>†</sup>

Center for Basic Science, National Renewable Energy Laboratory, 16253 Denver West Parkway, Golden, Colorado 80401, and Rochester Institute of Technology, 85 Lamb Memorial Drive, Rochester, New York, 14623

Received January 24, 2006. Revised Manuscript Received March 17, 2006

We present the first successful high-yield laser vaporization synthesis of high-quality boron-doped single-wall carbon nanotubes (B-SWNTs). Boron was loaded into graphite targets in the form of elemental B as well as nickel boride (NiB) and vaporized in a laser-oven apparatus in both Ar and N<sub>2</sub> ambients. Although targets containing elemental B produced no or low yields of SWNTs, the NiB catalyst in N<sub>2</sub> produced SWNT bundles comparable in quality to the best pure-carbon SWNTs produced from traditional Ni/Co catalysts. A variety of different samples were analyzed by transmission electron microscopy, Raman spectroscopy, X-ray diffraction, and nanoprobe electron energy loss spectroscopy (EELS). Boron was found to be doped substitutionally in the SWNT lattice at contents up to 1.8 at % by EELS. The <sup>13</sup>C NMR chemical shift of SWNT nuclei is affected by boron doping by shifting to higher frequency, as expected for p-type doping. The EELS and NMR data exclude the possibility of B and N codoping. Aspects of the growth mechanism are discussed.

## 1. Introduction

Carbon single-wall nanotubes (C-SWNTs) are essentially graphitic quantum wires that possess unique optical and electronic properties that arise from two-dimensional quantum confinement. As such, the density of states (DOS) of SWNTs is determined by the tube diameter and helicity. Attempts to utilize SWNTs as sensors, field-effect transistors, in electro-optic applications, and as gas storage media will likely require further control over structural, electronic, and optical properties via doping. For example, a recent theoretical calculation predicted that B incorporated within sp<sup>2</sup>-bonded carbon networks will strongly interact with hydrogen molecules via a Kubas-type interaction.<sup>1</sup> Considerable progress has been made with chemical<sup>2,3</sup> and electrochemical<sup>4</sup> methods using a wide variety of donors and acceptors to produce doping via charge-transfer interactions with nanotube surfaces. However, for many devices, it will be desirable to produce doped SWNTs in which dopant atoms are incorporated directly into the nanotube lattice. Progress in this area of research has been more limited.

Analogous to solid-state doping in semiconductors such as silicon, nanotubes can be made n-type by doping with electron-rich atoms such as nitrogen and p-type by doping with electron-deficient atoms such as boron. The properties

of doped SWNTs vary as a function of doping level, with changes expected at very low doping levels of <1%. As the doping level increases, mid-gap donor or acceptor levels may begin to control electronic properties such as transport and recombination.<sup>5</sup> Stoichiometric layered materials, such as BC<sub>2</sub>N, BC<sub>3</sub>, and C<sub>3</sub>N<sub>4</sub>, have been predicted to form nanotubes and in some cases have been successfully synthesized.<sup>6–9</sup>

The synthesis of B- and N-doped SWNTs (B-SWNTs and N-SWNTs) may be separated into two broad categories: postsynthetic processing and direct doping. In postsynthetic preparations, previously synthesized carbon nanotubes are mixed with dopant molecules or elements and reacted at very high temperatures to induce substitution of dopant atoms onto the carbon nanotube lattice. For example, one of the more popular preparations for B-SWNTs is the high temperature (>1200 °C) thermochemical reaction of pristine SWNTs with B<sub>2</sub>O<sub>3</sub>.<sup>6,10–13</sup> Although this method has been shown to produce high levels of B-doping, heterogeneity in the doping level

\* To whom correspondence should be addressed. E-mail: jeffrey\_blackburn@nrel.gov. Fax: 303-384-6655.

<sup>†</sup> National Renewable Energy Laboratory.

<sup>‡</sup> Rochester Institute of Technology.

- (1) Kim, Y.-H.; Zhao, Y.; Williamson, A.; Heben, M. J.; Zhang, S. B. *Phys. Rev. Lett.* **2006**, *96*, 016102.
- (2) Fischer, J. E. *Acc. Chem. Res.* **2002**, *35*, 1079.
- (3) Skakalova, V.; Kaiser, A. B.; Dettlaff-Weglikowska, U.; Hrnčarikova, K.; Roth, S. *J. Phys. Chem. B* **2005**, *109*, 7174.
- (4) Kavan, L.; Rapta, P.; Dunsch, L.; Bronikowski, M. J.; Willis, P.; Smalley, R. E. *J. Phys. Chem. B* **2001**, *105*, 10764.

- (5) Carroll, D. L.; Redlich, P.; Blase, X.; Charlier, J. C.; Curran, S.; Ajayan, P. M.; Roth, S.; Rühle, M. *Phys. Rev. Lett.* **1998**, *81*, 2332.
- (6) Fuentes, G. G.; Borowiak-Palen, E.; Knupfer, M.; Pichler, T.; Fink, J.; Wirtz, L.; Rubio, A. *Phys. Rev. B: Condens. Matter Mater. Phys.* **2004**, *69*, 245403/1.
- (7) Chopra, N. G.; Zettl, A. *Fullerenes* **2000**, 767.
- (8) Miyamoto, Y.; Rubio, A.; Cohen, M. L.; Louie, S. G. *Phys. Rev. B: Condens. Matter Mater. Phys.* **1994**, *50*, 4976.
- (9) Weng-Sieh, Z.; Cherrey, K.; Chopra, N. G.; Blase, X.; Miyamoto, Y.; Rubio, A.; Cohen, M. L.; Louie, S. G.; Zettl, A.; Gronsky, R. *Phys. Rev. B: Condens. Matter Mater. Phys.* **1995**, *51*, 11229.
- (10) Golberg, D.; Bando, Y.; Han, W.; Kurashima, K.; Sato, T. *Chem. Phys. Lett.* **1999**, *308*, 337.
- (11) Han, W.; Bando, Y.; Kurashima, K.; Sato, T. *Appl. Phys. Lett.* **1998**, *73*, 3085.
- (12) Han, W.; Bando, Y.; Kurashima, K.; Sato, T. *Chem. Phys. Lett.* **1999**, *299*, 368.
- (13) Golberg, D.; Bando, Y.; Bourgeois, L.; Kurashima, K.; Sato, T. *Carbon* **2000**, *38*, 2017.

can be a problem,<sup>6</sup> and many side products may form, including cages and large nanorods.<sup>13,14</sup> In direct doping, in contrast, boron- and/or nitrogen-containing reactants are mixed with the carbon and catalyst sources from which the nanotubes are grown. Several synthetic routes have explored the direct synthesis of B- and N-SWNTs, including arc discharge,<sup>5,9,15</sup> chemical vapor deposition (CVD),<sup>16–20</sup> and laser ablation.<sup>21–24</sup> Of these approaches, the CVD method has demonstrated the most success at producing nanotubes with significant levels of doping. To date, CVD has produced multiwall nanotubes (MWNTs) with widely varying structures and morphologies, but doped SWNTs have not been made.

Because the laser vaporization method is generally recognized for producing SWNTs of very high purity and low defect density,<sup>25,26</sup> it is desirable to produce B-SWNTs by this method. Although efforts to directly dope SWNTs with B using laser vaporization have produced some SWNTs, doping levels are typically below detection levels.<sup>21–24</sup> The work to date has attempted to use B, BN, and B<sub>4</sub>C as catalysts for nanotube growth by including these compounds into the graphite laser ablation target. In general, the quality of the SWNT product was observed to decrease as the concentration of B was increased, with no direct evidence for B incorporation into any nanotubes.<sup>21–23</sup> In fact, a very recent laser vaporization study showed that SWNT growth was inhibited when the B concentration in the target was above 3%. The resulting soot contained very few SWNTs, and the level of B incorporation was below the limit of detection in all cases.<sup>21</sup> A similar study utilized B, BN, and B<sub>4</sub>C dopants, without other metal catalysts, and found a low yield for SWNT and double-wall nanotubes (DWNTs) with, once again, no observable B incorporation into the lattice.<sup>23</sup>

Because transition metals provide the optimum catalysis for pure C-SWNT growth, it is reasonable to expect that B incorporation along with Ni and Co particles might assist in the successful knitting of B into the SWNT lattice. However, in syntheses in which Ni and Co metals were incorporated

**Table 1. Abbreviations Used for Laser Samples Prepared from Different Targets<sup>a</sup>**

sample name	Ni at %	Co at %	B at %	NiB mol %	C at %
Ni0.6/Co0.6	0.6	0.6			98.8
Ni0.6/Co0.6/B11	0.6	0.6	11		87.8
Ni11/B11	11		11		78
NiB–5				5	95
NiB–11				11	89

<sup>a</sup> The table lists the atomic percentage of each component that was mixed into each target. For example, the Ni11/B11 target was prepared from 11 at % Ni, 11 at % B, and 78 at % C.

into the target along with elemental B, the B incorporation was found to poison the reaction and inhibit nanotube growth.<sup>21</sup>

In this contribution, we describe the use of nickel boride (NiB) as a novel catalyst for growing boron-doped SWNTs by laser vaporization. In contrast to studies with other catalysts, we find that NiB does not compromise the quality or the yield of nanotubes in comparison to those of pure C-SWNTs. This work draws upon the recent success of the synthesis of BN nanotubes from the direct plasma nitridation of iron borides.<sup>27</sup> These experiments demonstrated that the liquid flow of the boride near the eutectic temperature allows for the extrusion of boron out of the alloy particle and into a hexagonal BN framework. In our syntheses, we doped carbon targets with varying levels of NiB, and for comparison with other studies in the literature, we also performed growth experiments with targets containing elemental B. Targets in which elemental B was incorporated produced either no SWNTs or very low yields of SWNTs, with little or no B incorporation, as determined by nanoprobe electron energy loss spectroscopy (EELS). It was found that laser vaporization of NiB-incorporated targets at 1175 °C in N<sub>2</sub> gas produced high yields of B-SWNTs with B concentrations in the range of ~1–2 at %. Laser vaporization of the same targets in Ar gas produced SWNTs in high yields but with much lower B concentrations. We studied these materials by transmission electron microscopy (TEM), Raman spectroscopy, X-ray diffraction, EELS, and <sup>13</sup>C NMR spectroscopy. The results obtained from these investigations allow us to speculate on the growth mechanism for the B-SWNTs.

## 2. Experimental Section

Target materials for laser vaporization were made by ball-milling the appropriate catalyst(s) with graphite (Alfa-Aesar, 5–10 μm) for 30 min in air. C-SWNTs were produced from graphite targets with ~0.6 at % each of Ni and Co powder. Attempts to make B-SWNTs involved loading either NiB (GFS Chemicals) or combinations of Ni, Co, and elemental B into the predominantly graphite target. Table 1 lists the target compositions used in this study. For convenience, samples are named according to the makeup (at %) of the target from which they were produced and the background gas in which the synthesis was performed. For example, two NiB-containing targets were employed, one with 18% NiB by mass (with graphite being the only other constituent) and one with 38% NiB by mass. These target materials contained final B loadings of 5 and 11 at %. Samples prepared from these targets in N<sub>2</sub> are

- (14) Golberg, D.; Bando, Y.; Sato, T.; Grobert, N.; Reyes-Reyes, M.; Terrones, H.; Terrones, M. *J. Chem. Phys.* **2002**, *116*, 8523.
- (15) Redlich, P.; Loeffler, J.; Ajayan, P. M.; Bill, J.; Aldinger, F.; Rühle, M. *Chem. Phys. Lett.* **1996**, *260*, 465.
- (16) Sen, R.; Satishkumar, B. C.; Govindaraj, A.; Harikumar, K. R.; Raina, G.; Zhang, J.-P.; Cheetham, A. K.; Rao, C. N. R. *Chem. Phys. Lett.* **1998**, *287*, 671.
- (17) Liu, J.; Webster, S.; Carrol, D. L. *J. Phys. Chem. B* **2005**, *109*, 15769.
- (18) Terrones, M.; Benito, A. M.; Manteca-Diego, C.; Hsu, W. K.; Osman, O. I.; Hare, J. P.; Reid, D. G.; Terrones, H.; Cheetham, A. K.; et al. *Chem. Phys. Lett.* **1996**, *257*, 576.
- (19) Yu, J.; Bai, X. D.; Ahn, J.; Yoon, S. F.; Wang, E. G. *Chem. Phys. Lett.* **2000**, *323*, 529.
- (20) Yu, J.; Ahn, J.; Yoon, S. F.; Zhang, Q.; Rusli; Gan, B.; Chew, K.; Yu, M. B.; Bai, X. D.; Wang, E. G. *Appl. Phys. Lett.* **2000**, *77*, 1949.
- (21) Gai, P. L.; Stephan, O.; McGuire, K.; Rao, A. M.; Dresselhaus, M. S.; Dresselhaus, G.; Colliex, C. *J. Mater. Chem.* **2004**, *14*, 669.
- (22) McGuire, K.; Gothard, N.; Gai, P. L.; Dresselhaus, M. S.; Sumanasekera, G.; Rao, A. M. *Carbon* **2005**, *43*, 219.
- (23) Hirahara, K.; Suenaga, K.; Bandow, S.; Iijima, S. *Chem. Phys. Lett.* **2000**, *324*, 224.
- (24) Zhang, Y.; Gu, H.; Suenaga, K.; Iijima, S. *Chem. Phys. Lett.* **1997**, *279*, 264.
- (25) Dillon, A. C.; Gennett, T.; Jones, K. M.; Alleman, J. L.; Parilla, P. A.; Heben, M. J. *Adv. Mater.* **1999**, *11*, 1354.
- (26) Dillon, A. C.; Parilla, P. A.; Alleman, J. L.; Gennett, T.; Jones, K. M.; Heben, M. J. *Chem. Phys. Lett.* **2005**, *401*, 522.

- (27) Loh, K. P.; Lin, M.; Yeadon, M.; Boothroyd, C.; Hu, Z. *Chem. Phys. Lett.* **2004**, *387*, 40.

named NiB-5:N<sub>2</sub> and NiB-11:N<sub>2</sub>, respectively. Samples were also prepared with 11 at % NiB, for which the carbon fraction was enriched with 20% <sup>13</sup>C (Cambridge Isotope Laboratories, Inc.) to study the effect of B doping on the SWNT <sup>13</sup>C NMR shift. This sample is denoted as <sup>13</sup>C-NiB-11. The <sup>13</sup>C NMR spectra were collected as recently described.<sup>28</sup>

Targets were made by pressing 5 g of material at 10 000 psi in a cylindrical die 1 in. in diameter, mounting it in a molybdenum holder, and positioning it into a quartz tube surrounded by a clamshell furnace. The furnace temperature during synthesis was 1175 °C. Argon and nitrogen were utilized separately as background gases at a pressure of 500 Torr and a flow rate of 100 cm<sup>3</sup>/min. Samples were vaporized with a pulsed alexandrite laser, running in the free mode at 10 Hz, which produces emission ~200 ns in duration. Laser power ranged from ~2 to 4 W at power densities of ~45–65 W/cm<sup>2</sup> in order to remain in a vaporization regime.<sup>26,29</sup> Material was produced at a rate of ~30 mg/h and collected in the cold zone downstream of the furnace.

Raw soots were purified in a manner similar to that reported previously.<sup>25</sup> Briefly, ~100 mg of raw soot was refluxed in 180 mL of 3 M nitric acid for 16 h. The material was filtered through a 0.2 μm PTFE filter, washed with water several times, and then washed successively with acetone and water until the filtrate became clear. Finally, the sample was washed with ~15 mL of 1 M potassium hydroxide, followed by water, until the filtrate became clear. The resulting paper was oxidized in static air at 500–520 °C.

TEM images and EELS data were taken in a Tecnai TF20-UT microscope equipped with a Gatan Image Filtering (GIF) system operating at 200 kV. Focused beam diameters ranging from 20 to 80 nm were utilized to study selected bundles. The EELS measurements were performed in the diffraction mode with a camera length of 1.2 M at an energy resolution of ~1.2 eV.

X-ray diffraction (XRD) was performed on a Scintag PTS four-circle goniometer (Bragg–Brentano geometry) using Cu Kα radiation (0.15406 nm) generated at 45 kV and 36 mA and detected with a liquid-nitrogen-cooled solid-state germanium detector with single-channel analyzer electronics. The source slits were 2.0 and 4.0 mm slits at a 290 mm goniometer radius, and the detector slits were 0.5 and 0.3 mm at the same radius. The scan rate was 0.12°/min from 1.5 to 101.5° 2θ in 0.03° steps.

Raman spectra were obtained as previously described<sup>26</sup> using 7 mW of 2.54 eV (488 nm) laser excitation. The slit width was 0.1 mm, allowing for a resolution of 2–4 cm<sup>-1</sup> across the measured spectrum. All spectra were taken under identical conditions and were not normalized. Slight differences in collection efficiency and surface roughness from sample to sample prohibit rigorous comparison of absolute intensities. However, qualitative assessments and comparison of spectral features within a given spectra can still be made with confidence.

High-resolution, solid-state <sup>13</sup>C NMR spectra were collected on a Bruker Avance 200 MHz spectrometer (4.7 T) operating at 50.13 MHz for <sup>13</sup>C at room temperature, with MAS rotation rates of 6 or 7 kHz under a nitrogen atmosphere, as recently described.<sup>28</sup>

**Caution:** The primary safety hazard involved with synthesizing SWNTs by laser vaporization is the laser itself, and the appropriate laser safety goggles should be worn at all times. Material handling should also be done with caution. SWNTs, and nanomaterials in general, should be considered a potential risk for dermal and

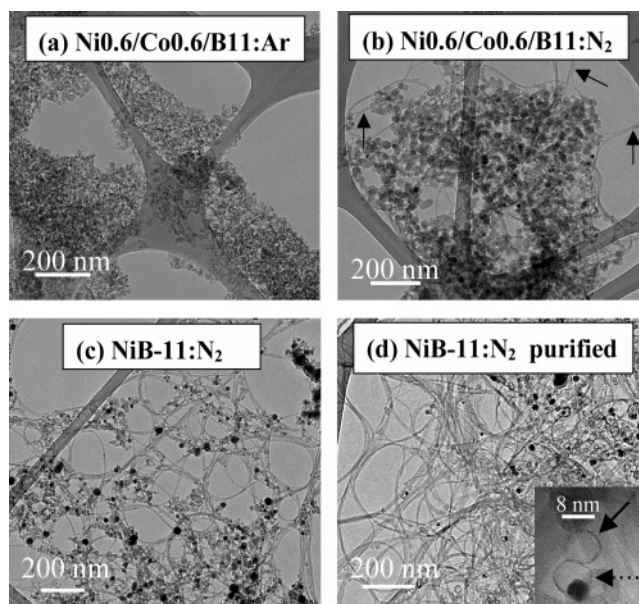


**Figure 1.** TEM images of soots obtained by laser vaporization of different targets; refer to Table 1 for sample identification and Table 2 for a summary of the general trends observed for all of the samples studied. Arrows in (b) show SWNT bundles. Inset in (d) shows high-magnification TEM image of the purified NiB-11 sample, showing onion-encapsulated nanoparticle (dashed arrow) and empty multiwalled cage (solid arrow).

pulmonary health effects. It is strongly advised such generated materials be handled with gloves and with the use of an appropriate respirator.

### 3. Results and Discussion

**3.1. Determining SWNT Content and B Incorporation with TEM, Raman, X-ray Diffraction, and EELS.** TEM and Raman spectroscopy are complimentary tools for evaluating SWNT content in raw soots. TEM allows for the direct imaging of SWNTs, amorphous carbon, nanocrystalline graphite, and residual catalyst particles but is generally not quantitative without extensive analysis. In contrast, Raman spectroscopy probes for SWNT content on the basis of the intensity and line shape of the various Raman signals. Coupling of the Raman excitation to electronic transitions of the SWNTs leads to a resonance enhancement for the SWNT modes that is not found for the other carbonaceous components. Thus, as the SWNT yield increases, the resonantly enhanced modes specific to the SWNTs “grow in” and predominate over a background of broad modes associated with non-nanotube carbon. For example, a multi-peak G band at high frequency and the radial breathing modes (RBMs) at low frequency are completely unique to SWNTs. Also, SWNTs have a unique multi-peak structure in the D band region of the spectrum that is not found for nanocrystalline graphite and amorphous carbon.<sup>30</sup>

TEM images (Figure 1) and Raman spectra (Figure 2) were obtained from samples produced under the different synthetic conditions to evaluate and compare the SWNT contents. The material generated from a target containing elemental boron, nickel, and cobalt mixed with graphite (Ni0.6/Co0.6/B11) with two different background gases, Ar and N<sub>2</sub>, are

(28) Engtrakul, C.; Davis, M. F.; Gennett, T.; Dillon, A. C.; Jones, K. M.; Heben, M. J. *J. Am. Chem. Soc.* **2005**, *127*, 17548.

(29) Dillon, A. C.; Parilla, P. A.; Alleman, J. L.; Perkins, J. D.; Heben, M. J. *Chem. Phys. Lett.* **2000**, *316*, 13.

(30) Dillon, A. C.; Yudasaka, M.; Dresselhaus, M. S. *J. Nanosci. Nanotechnol.* **2004**, *4*, 691.

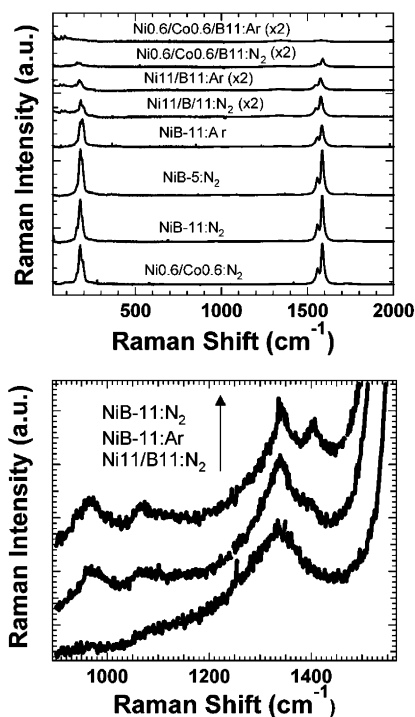


**Figure 2.** (a) Raman spectra of raw laser soots made from all of the target compositions explored in this study. The carrier gas for each sample is denoted after the sample ID. The excitation wavelength was 488 nm. The same power density was used for all samples. Refer to Table 1 for sample identification. All RBM modes are multiplied by 10 for clarity, and the higher frequency tangential regions for the top four spectra are multiplied by 2, as noted in the figure. The small peaks in some spectra below  $100\text{ cm}^{-1}$  are artifacts due to incomplete excitation filtering and are not SWNT modes. (b) Enlargement of the D band region for three samples, showing the evolution of fine structure as the SWNT yield increases

displayed in panels a and b, respectively, of Figure 1. No SWNTs were formed in Ar (Figure 1a). The sample consists of a mixture of amorphous carbon, nanocrystalline graphite, and metal catalyst particles. These findings are consistent with the results of a recent study that performed an identical experiment.<sup>21</sup> In  $\text{N}_2$ , however, the same target mixture produces a low yield of SWNT bundles (Figure 1b, arrows) that extend through and between large patches of amorphous and nanocrystalline graphite impurities.

Raman measurements (Figure 2) confirm what is seen by TEM. The  $\text{Ni}_{0.6}/\text{Co}_{0.6}/\text{B}_{11}:\text{Ar}$  sample shows no evidence of the G band or RBM modes indicative of SWNTs, although these modes are clearly evident when the same target is vaporized in  $\text{N}_2$ . Although the yield of SWNTs in  $\text{N}_2$  is somewhat low, the fact that we observe any SWNT formation at all for the  $\text{Ni}_{0.6}/\text{Co}_{0.6}/\text{B}_{11}:\text{N}_2$  sample is significant. Gai et al. proposed that B loadings greater than 3 at % in the target poisoned Ni/Co catalyst particles in Ar such that SWNT growth was prevented.<sup>21</sup> Analysis of the poisoned catalysts by EELS found particles with a high boron-to-metal ratio (B:M) of 5–20 and many boron carbide ( $\text{B}_4\text{C}$ ) particles.<sup>21</sup> Our results show that the formation of SWNTs at a high boron loading of 11 at % (B:M  $\approx$  9) is possible in a nitrogen atmosphere, suggesting that  $\text{N}_2$  perturbs the distribution of B during vaporization such that SWNT growth is permitted.

Following the idea that a high B:M ratio inhibits SWNT growth, we attempted to reduce the B:M ratio of particles

generated by the laser by increasing the loading of the transition metal component. To simplify, we eliminated Co and prepared targets with equal amounts of B and Ni (B:M = 1) using elemental Ni and B powders ( $\text{Ni}_{11}/\text{B}_{11}$ ). Samples produced with the  $\text{Ni}_{11}/\text{B}_{11}$  target were slightly improved over the  $\text{Ni}_{0.6}/\text{Co}_{0.6}/\text{B}_{11}$  samples (B:M  $\approx$  9) in both Ar and  $\text{N}_2$ . A relatively low yield of SWNTs was found by TEM for the  $\text{Ni}_{11}/\text{B}_{11}:\text{Ar}$  sample (data not shown), but Raman spectroscopy showed a strong G band feature in contrast to the  $\text{Ni}_{0.6}/\text{Co}_{0.6}/\text{B}_{11}:\text{Ar}$  sample. The Raman spectra of the  $\text{Ni}_{11}/\text{B}_{11}:\text{N}_2$  sample also indicated a substantial increase in tube content relative to the  $\text{Ni}_{11}/\text{B}_{11}:\text{Ar}$  data (Figure 2).

Growth experiments were also performed with targets loaded with the compound NiB to obtain a 1:1 B:M ratio without using the elements. Surprisingly, the SWNT yields were dramatically improved relative to when Ni and B were incorporated in the elemental form. Figure 1c displays a TEM image of the high-quality material produced from a  $\text{NiB-11}:\text{N}_2$  target. The Raman spectra from several samples produced from NiB-doped targets are shown in Figure 2. We first note that the  $\text{NiB-5}:\text{N}_2$  and  $\text{NiB-11}:\text{N}_2$  spectra are much more intense than the  $\text{Ni}_{11}/\text{B}_{11}:\text{N}_2$  spectrum, making it clear that SWNT formation is favored when B is incorporated via NiB rather than via elemental Ni and B. Also, the Raman signals for the  $\text{NiB-11}:\text{Ar}$  sample are significantly enhanced relative to the  $\text{Ni}_{11}/\text{B}_{11}:\text{Ar}$  data but substantially weaker than the  $\text{NiB-11}:\text{N}_2$  modes. Thus, the previously discussed observation that  $\text{N}_2$  is better than Ar for SWNT production using elemental B and Ni is also found when NiB is employed. Finally, we point out that the  $\text{NiB-5}:\text{N}_2$  and  $\text{NiB-11}:\text{N}_2$  Raman modes are similar in intensity to the signals from optimized  $\text{Ni}_{0.6}/\text{Co}_{0.6}:\text{N}_2$  SWNTs, which are known to be very high quality SWNT samples.<sup>25,26</sup> This is striking considering that the initial metal loading in the NiB targets is much higher. Such a high production yield of SWNTs from targets with a high boron loading is unprecedented.

The B-SWNTs are easily purified by 16 h of nitric acid reflux and air oxidation.<sup>25</sup> Figure 1d shows a TEM image of the purified  $\text{NiB-11}$  sample produced in  $\text{N}_2$ . The sample consists of clean SWNTs, free of amorphous carbon, with some carbon cages. Some cages are empty and some contain residual catalyst nanoparticles. The existence of these cages prohibits us from obtaining highly pure samples. Apparently, nitric acid may permeate through many of these cages, leaving empty graphitic shells, whereas many cages are impermeable such that graphite-encapsulated particles remain (Figure 1d, inset). Similar onion-encapsulated  $\text{B}_4\text{C}$  particles were observed in previous B laser vaporization studies.<sup>21</sup>

The quality of the material may also be seen in the D band region of the Raman spectrum from  $\sim 1300$  to  $1420\text{ cm}^{-1}$ . Figure 2b shows the broad, featureless D band from the  $\text{Ni}_{11}/\text{B}_{11}:\text{N}_2$  sample, as expected for a relatively low SWNT content and high concentrations of amorphous carbon or nanocrystalline graphite. The SWNT yield increases when the  $\text{NiB-11}$  target is vaporized in Ar, and the D band fine structure, which is due to a double-resonance process,<sup>31</sup> begins to emerge. The D band region is dominated by the SWNT fine structure when the  $\text{NiB-11}$  target is employed

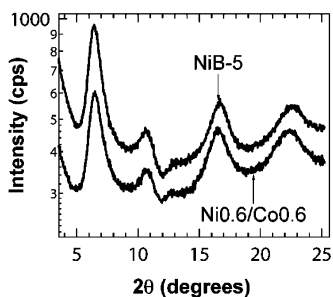


**Figure 3.** Low-angle X-ray diffraction patterns for (top) a boron-doped SWNT sample, NiB-5, and (bottom) a C-SWNT sample, Ni<sub>0.6</sub>/Co<sub>0.6</sub>, showing the reflections arising from SWNT bundles.

in N<sub>2</sub>, indicating both a high yield as well as a low defect density for these laser-generated B-SWNTs.<sup>30</sup> The quality of the SWNTs produced by the NiB catalyst in N<sub>2</sub> is also evident in the X-ray data of Figure 3. Here, the reflections associated with bundled nanotubes are compared for the NiB-5:N<sub>2</sub> and Ni<sub>0.6</sub>/Co<sub>0.6</sub>:N<sub>2</sub> samples. The X-ray patterns are offset for clarity and show that large concentrations of well-bundled SWNTs are present in both samples.

Nanoprobe EELS measurements were employed to determine the local B content and B bonding geometry in B-SWNT bundles and to identify which growth parameters permitted the incorporation of B into the SWNT lattice. The B-SWNT composition and bonding information was obtained by ensuring that the EELS probe examined only clean bundles that were well-separated from other non-nanotube fractions in the sample. Figure 4 displays TEM images of isolated SWNT bundles (Figure 4a–c) and associated EELS spectra (Figure 4d–f) for high-quality samples produced from the NiB catalyst. Clean SWNT bundles were observed for the NiB-11 target vaporized in Ar (Figure 4a), and the EELS spectrum shows the characteristic core-level excitations at 188 and 284 eV for boron and carbon, respectively (Figure 4d). The B signal (Figure 4d, inset) is at the limit of detection and lacks the well-defined 1s → π\* resonance at 192 eV associated with B in an sp<sup>2</sup> hexagonal lattice. The 1s → σ\* resonance at ~199 eV that would be expected for other crystalline phases containing B is also not clearly observed. Consequently, the B detected here is likely distributed in a small amount of amorphous material in or on the SWNT bundle, although low levels of B may also be doped into the nanotube lattice. The B:C ratio for this sample is estimated to be in the range of ~0–0.2 at %.

In contrast, the NiB-5:N<sub>2</sub> sample (Figure 4b,e) clearly shows EELS fine structure in the B region that is attributed to the 1s → π\* resonance at 192 eV and the 1s → σ\* resonance at ~199 eV, as expected for sp<sup>2</sup>-bonded B (inset). The EELS structure is similar to that seen for multiwall boron nitride nanotubes and is direct evidence for incorporation of B into the hexagonal nanotube lattice.<sup>6,32</sup> The B:C ratio for this particular bundle is ~1.0 at %, whereas the analysis of several bundles from this sample yielded a B:C range of ~0.20–1.2 at %.

The EELS data for the NiB-11:N<sub>2</sub> sample shows that the amount of B incorporated into the nanotubes increases as the concentration of NiB is increased in the target (Figure 4c,f). Integration of the EELS spectrum yields a B:C ratio of 1.7 at %, whereas the range of the B:C ratio from bundle to bundle was ~0.8–1.8 at %. Again, the most striking features are the sharp, well-defined 1s → π\* and 1s → σ\* resonances that confirm we have achieved true substitutional doping of B into the SWNT lattice.

Although a sharp B 1s → π\* resonance at ~192 eV is typically used as evidence for incorporation of B into a nanotube lattice, it is often not appreciated or discussed that other impurities may give rise to such a peak. For example, this peak is observed for hexagonal boron nitride (h-BN), highly crystalline boron carbide (B<sub>4</sub>C), and for the NiB catalyst particles.<sup>33,34</sup> One must also consider that the 1s → π\* peak for boron oxide at 194 eV is very close to the 1s → π\* signal for sp<sup>2</sup>-bonded B at 192 eV.<sup>35</sup> Once again, we note that these nanoprobe EELS measurements were performed on very clean, well-formed SWNT bundles. The strong, sharp bundle peaks observed in the previously discussed XRD patterns suggest the absence of significant quantities of crystalline impurities trapped within the bundles, as these phases would disrupt the integrity of the bundles and affect the XRD spectrum. Thus, the well-defined bundle structure observed by TEM, as well as the XRD data shown in Figure 3, suggest close-packed SWNTs within the bundles and the absence of significant amounts of trapped crystalline NiB, BN, B<sub>4</sub>C, or B<sub>2</sub>O<sub>3</sub>. The absence of BN and B<sub>2</sub>O<sub>3</sub> may also be confirmed by the EELS spectra. The lack of a nitrogen signal near 400 eV or an oxygen signal near 500 eV eliminates the possibility of the observed 1s → π\* signal being due to h-BN or B<sub>2</sub>O<sub>3</sub>, respectively. Finally, as previously discussed with respect to the data in panels a and d of Figure 4, we note that crystalline rather than amorphous phases must be responsible for the observed fine structure. Consequently, the data are not accounted for by non-nanotube amorphous B-containing phases that could possibly be trapped within or decorated on top of the SWNT bundles.

For completeness, we note that the targets with elemental B that produced SWNTs in low yields showed little B incorporation in EELS experiments. Small amounts of amorphous B were seen for the Ni11/B11 sample in Ar, and small amounts of amorphous and sp<sup>2</sup>-bonded B were seen for the Ni11/B11 sample in N<sub>2</sub>. The distribution of B in samples made with the Ni11/B11 targets varied significantly from bundle to bundle.

The observation that N<sub>2</sub> assists in B incorporation when NiB is used in the target suggests the possibility of nitrogen codoping to form regions of stoichiometry near C<sub>2</sub>BN.<sup>36,37</sup> To examine this possibility, we first inspected the N region

(31) Zolyomi, V.; Kurtl, J.; Gruneis, A.; Kuzmany, H. *Phys. Rev. Lett.* **2003**, *18*, 157401.

(32) Fuentes, G. G.; Borowiak-Palen, E.; Pichler, T.; Liu, X.; Graff, A.; Behr, G.; Kalenczuk, R. J.; Knupfer, M.; Fink, J. *Phys. Rev. B: Condens. Matter Mater. Phys.* **2003**, *67*, 035429/1.

(33) Jimenez, I.; Jankowski, A. F.; Terminello, L. J.; Sutherland, D. G. J.; Carlisle, J. A.; Doll, G. L.; Tong, W. M.; Shuh, D. K.; Himpsel, F. J. *Phys. Rev. B: Condens. Matter Mater. Phys.* **1997**, *55*, 12025.

(34) McIlroy, D. N.; Zhang, D.; Cohen, R. M.; Wharton, J.; Geng, Y.; Norton, G.; De Stasio, G.; Gilbert, B.; Perfetti, L.; Streiff, J. H.; Broocks, B.; McHale, J. L. *Phys. Rev. B: Condens. Matter* **1999**, *60*, 4874.

(35) Borowiak-Palen, E.; Pichler, T.; Graff, A.; Kalenczuk, R. J.; Knupfer, M.; Fink, J. *Carbon* **2004**, *42*, 1123.

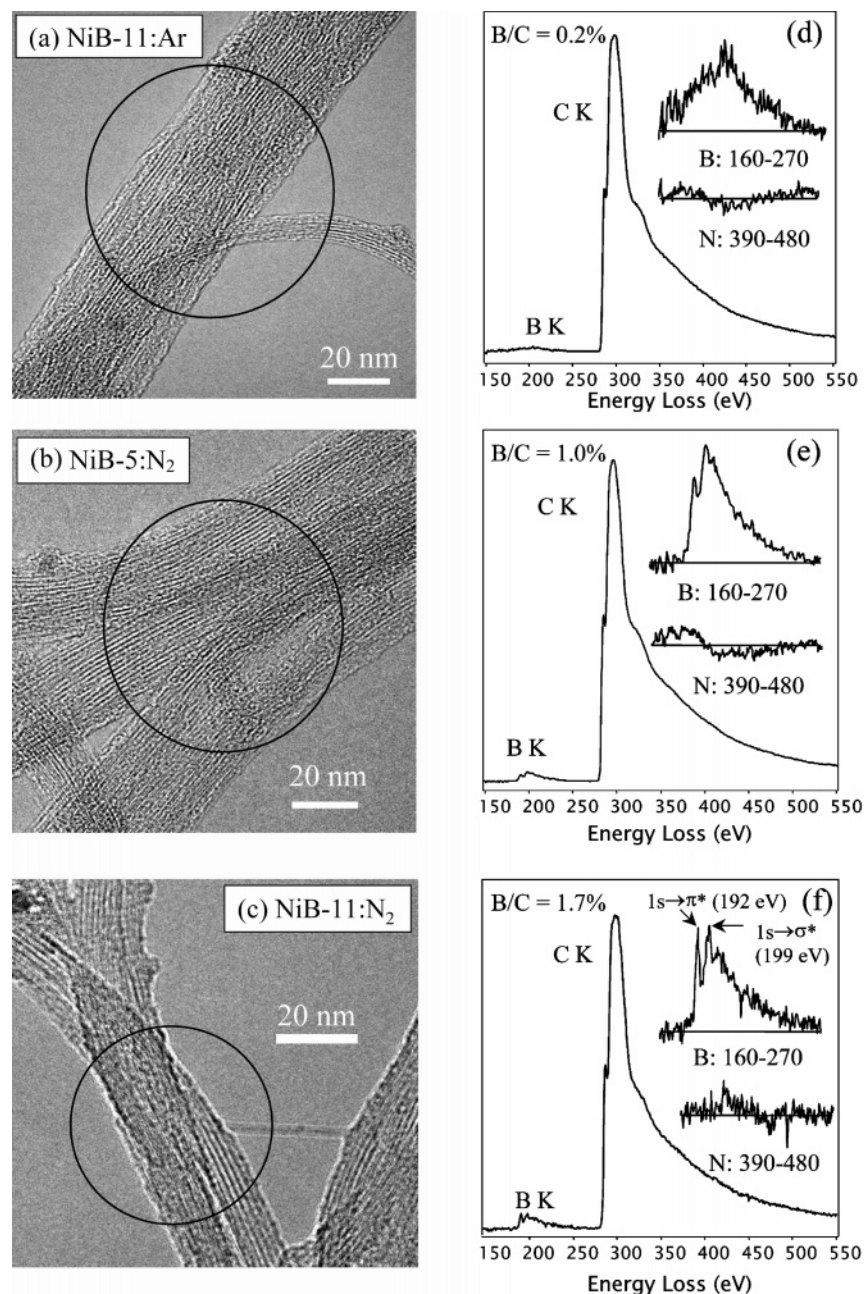


**Figure 4.** (a–c) High-magnification TEM images of representative SWNT bundles studied with nanoprobe EELS for NiB-11:Ar, NiB-5:N<sub>2</sub>, and NiB-11:N<sub>2</sub>, respectively. The circle in each figure represents the approximate area probed by the electron beam for EELS analysis. (d–f) EELS spectra for the circled areas shown in a–c, respectively. The insets show enlargements of the boron and nitrogen regions for each EELS spectrum.

in the EELS spectrum from the NiB-11 sample produced in Ar. As expected, no significant N was observed above the background associated with the large C signal (Figure 4d, inset). The positive and negative deviation of the N signal from the baseline originates from the method by which the C background was subtracted and is consistent with there being no detectable nitrogen. For comparison, the nitrogen EELS signals from samples produced in N<sub>2</sub> are shown in the insets of panels e and f of Figure 4. As with the sample produced in Ar, the signals in the N region are small, oscillatory, and barely detected above the background

noise. The Hartree–Slater model indicates that the ionization cross section for N is approximately  $1/5$  that of B. With the reduced sensitivity to N, we expect nitrogen contents of  $\sim 1$  at % to be readily measured. Considering a B:C ratio of  $\sim 1$ – $1.8$  at % observed for the NiB-11 sample, the lack of a readily observed N signal indicates that B and N are not codoped in a 1:1 ratio. However, we cannot exclude at this time the possibility that nitrogen may be incorporated into the SWNT lattice at low levels less than  $\sim 0.5$  at %.

We note that EELS spectra obtained from the purified NiB-11:N<sub>2</sub> sample (not shown) reveal an sp<sup>2</sup>-bonded B doping level of  $\sim 0.5$ – $1.0$  at %, significantly less than the 1.0–1.8 at % seen prior to purification. The lower B

(36) Kobayashi, K.; Kurita, N. *Phys. Rev. Lett.* **1998**, *70*, 3542.

(37) Watanabe, M. O.; Itoh, S.; Mizushima, K.; Sasaki, T. *Appl. Phys. Lett.* **1996**, *68*, 2962.

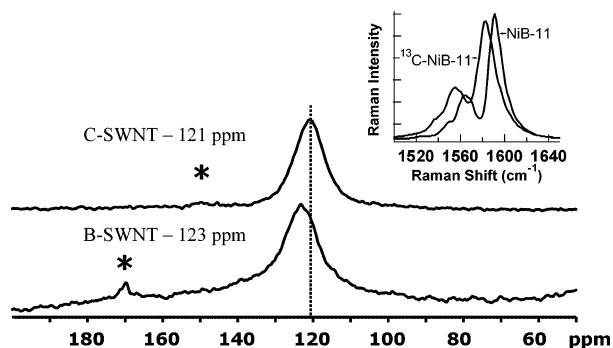


**Figure 5.**  $^{13}\text{C}$  NMR spectra for B-SWNT and C-SWNT. Both are enriched with 20%  $^{13}\text{C}$ . Inset shows Raman spectra of B-SWNT that is enriched with 20%  $^{13}\text{C}$  ( $^{13}\text{C}$ -NiB-11) and unenriched B-SWNT (NiB-11). Asterisks mark spinning sidebands.

concentration in the purified material suggests that some of the  $\text{sp}^2$ -bonded B in the SWNTs may have reacted in the highly oxidizing purification environments. Indeed, EELS spectra of the purified material clearly show structure in the oxygen region (edge  $\sim 500$  eV), indicating that the tubes become functionalized with oxygen-containing moieties during purification. Also, small amounts of B present as amorphous impurities that possibly contributed to the integrated B signal may have been removed by the purification.

**3.2.  $^{13}\text{C}$  NMR.** To further examine whether B is indeed incorporated into the SWNT lattice, we performed NMR experiments with B-SWNTs that were also enriched with 20 at %  $^{13}\text{C}$  ( $^{13}\text{C}$ -NiB-11: $\text{N}_2$ ). NMR has recently been shown to be a highly sensitive probe of the electronic environment for carbon nuclei in SWNTs.<sup>28</sup> Specifically, it was shown that removal of electron density from SWNTs by protonation led to a reproducible shift to higher frequency of the  $^{13}\text{C}$  resonance. Substitutional boron in a carbon lattice represents an electron-deficient atom, rendering the B-SWNTs p-type in electronic character. Consequently, B should reduce the  $\pi$  electron density of the SWNTs, as was observed for protonation.

Figure 5 compares the Raman spectra of the unenriched NiB-11: $\text{N}_2$  material to that of the  $^{13}\text{C}$ -NiB-11: $\text{N}_2$  sample in the region of the G band. Both materials were purified as previously described. The G band is observed to be shifted to lower frequency by  $8\text{ cm}^{-1}$ , as expected for 20% of the SWNT carbon being the heavier  $^{13}\text{C}$  atom.<sup>38</sup> Figure 5 also shows the NMR spectra for the same two samples. The top spectrum displays the  $^{13}\text{C}$  resonance for carbon nuclei in purified carbon SWNT at 121 ppm, whereas the bottom spectrum shows the NMR spectrum for the purified B-SWNTs that contain  $\sim 0.5$ – $1.0$  at % B. A clear shift of the  $^{13}\text{C}$  resonance to 123 ppm can be seen for the B-SWNTs, consistent with the removal of electron density from the  $\pi$  system, in agreement with previous work on SWNTs<sup>28</sup> and conducting polymers.<sup>39</sup> The magnitude of the shift may be rationalized by considering the NMR of SWNTs in a Nafion matrix, in which a 4 ppm shift to higher frequency was estimated to arise from a reduction in electron density of  $\sim 0.02\text{ e}^-/\text{C}$ .<sup>28</sup> Thus, the 2 ppm shift observed here corre-

sponds to a reduction in electron density of  $\sim 0.01\text{ e}^-/\text{C}$  due to B doping. Put differently, the data indicate that approximately 1 electron (hole) is removed (added) from the tube for every 100 carbon atoms. Interestingly, this estimate is in excellent agreement with the B doping level in these samples as determined by EELS ( $\sim 0.5$ – $1.0$  at %). Also, the fact that an NMR shift is observed at all suggests that codoping of BN species does not occur, in agreement with the EELS data in which N was not observed. Codoped BN species would not change the net electron density on the tube. These are the first measurements of a change in  $^{13}\text{C}$  resonance as a result of substitutional doping in SWNTs, which independently confirms the conclusion from EELS that B is indeed substitutionally doped into the SWNT lattice.

We stress that the NMR measurements were made possible by the purification process that removed a majority of the residual metal catalyst particles. When large amounts of catalyst particles remain in the sample, the isotropic  $^{13}\text{C}$  NMR signal for the SWNTs may be broadened and possibly washed out. Although catalyst particles were rigorously removed for the  $^{13}\text{C}$  NMR experiments discussed here, we have also investigated samples in which less residual catalyst was removed. Whereas these samples showed broader peaks than those that had the catalyst more thoroughly removed, the peak shifts were identical, confirming that the residual catalyst particles do not affect the  $^{13}\text{C}$  chemical shift.

**3.3. Growth Mechanism.** Table 2 summarizes the results for seven samples prepared with boron-doped targets. The overall observations may be summarized as follows. (1) Nitrogen increases the SWNT yield for all target compositions, (2) Targets with low transition metal loading and high B loading produce small quantities of SWNTs only in  $\text{N}_2$ . (3) Increasing the concentration of transition metals (Ni) relative to the concentration of elemental B increases the yield and quality of SWNTs. (4) The use of the NiB alloy as a SWNT catalyst results in high-quality B-SWNT bundles, comparable in quality to the best C-SWNTs produced from traditional Ni/Co catalysts. (5) Use of the NiB catalyst in  $\text{N}_2$ , as compared to Ar, permits higher and more-homogeneous B doping. These observations allow us to speculate on the growth mechanism of the B-SWNTs.

First, it is clear that nitrogen plays an important role in facilitating the growth of SWNTs when B is present. This role may be physical, in that collision rates, ionization efficiencies, thermal conductivities, or heat capacities vary enough between argon and nitrogen to change the plume temperature or temporal dynamics significantly. Recent studies of SWNT laser growth in Ar and  $\text{N}_2$  found that the higher thermal conductivity and heat capacity of  $\text{N}_2$  caused the carbon plume to cool more quickly, resulting in smaller-diameter tubes.<sup>40,41</sup> The role may also be chemical, in that chemical reactions involving nitrogen molecules/atoms/ions may change the overall chemical makeup of the species in the plume. Both physical and chemical factors likely contribute to the differences observed for B-SWNT produc-

(38) Liu, L.; Fan, S. S. *J. Am. Chem. Soc.* **2001**, *123*, 11502.

(39) Clarke, T. C.; Scott, J. C.; Street, G. B. *IBM J. Res. Dev.* **1983**, *27*, 313.

(40) Nishide, D.; Kataura, H.; Suzuki, K.; Tsukagoshi, K.; Aoyagi, Y.; Achiba, Y. *Chem. Phys. Lett.* **2003**, *372*, 45.

(41) Ikegami, T.; Nakanishi, F.; Uchiyama, M.; Ebihara, K. *Thin Solid Films* **2004**, *457*, 7.

**Table 2. Summary of Tube Density, Boron-to-Carbon Ratio (expressed as a percentage), and Overall Homogeneity of the Boron Distribution in the Bundles as a Function of Target Material and Carrier Gas**

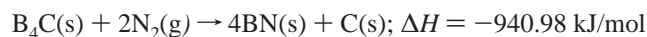
target material	carrier gas	tube density	B:C in tubes (at %)	distribution of B in tubes
Ni <sub>0.6</sub> /Co <sub>0.6</sub> /B11	Ar	no tubes	n.a. <sup>a</sup>	n.a. <sup>a</sup>
Ni <sub>0.6</sub> /Co <sub>0.6</sub> /B11	N <sub>2</sub>	low	0	n.a. <sup>a</sup>
Ni11/B11	Ar	very low	0–0.2	amorphous, heterogeneous
Ni11/B11	N <sub>2</sub>	low to medium	0–0.8	amorphous, sp <sup>2</sup> , heterogeneous
NiB-11	Ar	high	0–0.2	amorphous, heterogeneous
NiB-5	N <sub>2</sub>	high	0.2–1.2	sp <sup>2</sup> , more homogeneous
NiB-11	N <sub>2</sub>	high	0.8–1.8	sp <sup>2</sup> , more homogeneous
NiB-11 purified	N <sub>2</sub>	very high	0.5–1	sp <sup>2</sup> , more homogeneous

<sup>a</sup> n.a. = not applicable.

tion in N<sub>2</sub> and Ar. For this report, we restrict the discussion to potential chemical interactions, leaving open the possibility that physical interactions may also play a role.

Gai et al. previously noted that no SWNTs were produced by laser vaporization of targets with high boron-to-metal ratios. Instead, large amounts of B<sub>4</sub>C and nickel-enriched boron particles with B:M ratios greater than 5 were found.<sup>21</sup> Thus, we consider the suppression of these types of condensed phases to be essential for high-yield SWNT growth. Accordingly, it is useful to roughly distinguish between two types of metal particles that may be formed: (1) particles with B:M ≫ 1 (i.e., nickel-enriched boron particles), and (2) particles with B:M ≤ 1 (i.e., boron-enriched nickel particles). Although the former are likely poor SWNT catalysts,<sup>21</sup> the data presented here indicate that the latter are effective in producing SWNTs.

A N<sub>2</sub> background gas can be expected to suppress the formation of both nickel-enriched boron particles and boron carbide by serving as an additional reactant to drive the formation of boron nitride. Boron nitride may be directly formed via the bimolecular recombination of energetic B and N species in the plume, which would getter some B species and effectively decrease the average B:M ratio in potentially catalytic particles. Boron nitride could also be formed indirectly from the boron carbide particles observed previously via the well-known reaction of boron carbide in a nitrogen atmosphere



This exothermic reaction has a large negative free-energy change over a large temperature range ( $\Delta G = 0$  at 2485 °C)<sup>42</sup> and could free up carbon feedstock that might aid in SWNT formation. However, the amount of additional carbon available in N<sub>2</sub> would be small on a percentage basis, so the dominant beneficial effect of using N<sub>2</sub> in the laser synthesis is likely associated with a shift in the composition of catalytic species in the laser plume from nickel-enriched boron particles (B:M ≫ 1) to boron-enriched nickel particles (B:M ≤ 1).

A comparison of the data from samples produced from targets with the same elemental boron loading but very different transition metal loadings supports the idea that particles with a low B:M ratio are desired for SWNT formation. In Ar, the Ni11/B11 (B:M = 1) target produces SWNTs in significant quantities, whereas the Ni<sub>0.6</sub>/Co<sub>0.6</sub>/

B11 (B:M ≈ 9) target produces none. The composition of the particles in the gas phase that may serve as catalysts for growth is likely related to the composition of the target, as is the case for other SWNT syntheses. Thus, simply decreasing the B:M ratio in the target avoids “poisoning”<sup>20</sup> of the catalyst. The production of SWNTs in N<sub>2</sub> is enhanced for both targets because of a further decrease in the B:M ratio as a result of the previously discussed gas-phase chemistry.

The fact that the SWNT production yield is dramatically improved when the Ni and B are incorporated into the target as a compound rather than as the elements also supports the view that a low B:M ratio is desired. When Ni and B are evaporated as the elements in Ar, the difference in melting points for Ni and B (1430 vs 2180 °C) suggests that B and Ni would precipitate out of the energetic plume without appreciable alloying, leading to particles that are either primarily nickel (B:M ≪ 1) or primarily boron (B:M ≫ 1). A small number of particles with intermediate compositions might be formed depending on the degree to which the Ni and B particle/atom distributions could interact while cooling. Because the near-pure boron particles do not catalyze SWNT growth, the SWNT yield, due primarily to the nickel particles, is low compared to the Ni/Co catalyst employed for optimized C-SWNT growth. However, the fact that a small amount of B incorporation is observed by EELS raises the possibility that at least some B:M particles are active in SWNT growth. In contrast, when NiB (melting point 1590 °C) is vaporized from the target in Ar, a large fraction of the clusters in the gas phase are expected to have a composition near NiB. These particles are evidently quite efficient at knitting carbon to form SWNTs. However, though the SWNT yield is dramatically improved, the use of NiB versus elemental Ni and B (in Ar) does not appreciably improve the homogeneity or magnitude of B incorporation.

Similarly, NiB is much more effective in SWNT growth in N<sub>2</sub> than are the elements in the same 1:1 ratio. However, the use of N<sub>2</sub> increases the incorporation of B and improves the homogeneity of the B distribution from bundle to bundle. As stated earlier, the NiB11:N<sub>2</sub> sample is comparable in quality to the high-quality C-SWNT material prepared with the optimized Ni/Co catalyst. In this case, the gas-phase chemistry in N<sub>2</sub> leads to the possibility that the B:M ratio for catalytic particles in the plume may be reduced below unity. The Ni/B binary phase diagram shows several boron-rich nickel phases, such as Ni<sub>3</sub>B and Ni<sub>2</sub>B, and small particles of these would likely exist as liquid droplets at the growth

(42) Zhang, G. J.; Ando, M.; Yang, J. F.; Ohji, T.; Kanzaki, S. *J. Eur. Ceram. Soc.* **2004**, *24*, 171.

temperature of 1175 °C. Once  $C_x$  species were absorbed by the liquid alloy particles, it is reasonable to expect that B may be extruded along with the SWNT as it grows from the particle surface.<sup>27</sup> Thus, the creation of large amounts of active, boron-containing Ni-catalyst particles explains the very high SWNT yield and successful B incorporation associated with the NiB catalyst. This model is supported by the observation of a Ni<sub>2</sub>B X-ray diffraction signal in the best samples (data not shown).

The literature exploring C-SWNT production via laser vaporization in nitrogen gas is sparse, both theoretically and experimentally.<sup>40,41,43</sup> Recent studies report an increase in the C<sub>2</sub> "swan" band in a nitrogen atmosphere relative to the same type of target vaporized in an argon atmosphere.<sup>41</sup> Low-molecular-weight species, such as C<sub>2</sub>, have been shown to be essential precursors for nanotube growth.<sup>44</sup> More importantly for our work, CN species were observed in the plasma, indicating the direct chemical reaction of nitrogen and carbon species in the plume.<sup>41</sup> As discussed earlier, the recombination of B and N atoms in the plume may also occur when B is doped into laser targets. The presence of energetic BN species in the plasma could, similar to what happens with CN and C<sub>2</sub> species, facilitate the incorporation of B into catalyst particles and, subsequently, into the SWNT lattice. Excited BN species could also collide with nascent SWNTs, substituting B atoms or BN pairs into the SWNT lattice. These occurrences would only be likely for excited diatomic BN species that could be easily absorbed by the catalyst particles or impinge on growing SWNT walls; larger condensed BN particles are not expected to catalyze SWNT growth. Because codoping of BN pairs is not observed, the N atoms must be eliminated to some degree. Alternatively, nitrogen gas may interact at the interface of a B-rich catalyst

particle and emerging SWNT, stabilizing B at the interface so that substitutional incorporation of B is possible. Clearly, the mechanism responsible for the enhancement of B doping in a N<sub>2</sub> atmosphere is unclear and warrants future exploration. The system is quite complicated by virtue of the four elemental species present and the nonequilibrium nature of the laser synthesis experiments. Efforts aimed at analyzing the chemical makeup and real-time evolution of the laser-vaporized plume would greatly aid in elucidating the mechanism.

#### 4. Conclusion

High yields of boron-doped SWNTs were produced by the laser-vaporization process for the first time. Vaporization of graphite targets containing NiB in a nitrogen atmosphere produced high yields of high-quality SWNTs. Boron was found to be substitutionally doped into the SWNT lattice at levels up to ~1.8 at % by EELS. The NiB alloy is successful in producing B-SWNTs by suppressing the formation of particles with high B:M ratios. We present the first <sup>13</sup>C NMR analysis of B-SWNTs, which shows that the removal of electron density from the SWNT  $\pi$  electron system by electron-deficient B atoms leads to a 2 ppm shift of the <sup>13</sup>C resonance to higher frequency. These materials should be useful in a variety of applications requiring permanent modification of the chemical and electronic properties of SWNTs.

**Acknowledgment.** We thank Mark Davis for assistance with NMR experiments and Mowafak Al-Jassim for facilitating EELS measurements. This work was funded by the U.S. Department of Energy Office of Energy Efficiency and Renewable Energy Hydrogen Program and by the Office of Science, Basic Energy Sciences, Division of Materials Sciences and Engineering under Subcontract DE-AC36-99GO10337 to NREL.

(43) Zhang, Y.; Gu, H.; Iijima, S. *Appl. Phys. Lett.* **1998**, *73*, 3827.

(44) Scott, C. D.; Arepalli, S.; Nikolaev, P.; Smalley, R. E. *Appl. Phys. A* **2001**, *72*, 573.